Biosensors and Bioelectronics 126 (2019) 170–177

Contents lists available at ScienceDirect

Biosensors and Bioelectronics

journal homepage: www.elsevier.com/locate/bios

Significant enhancement of direct electric communication across enzyme-electrode interface *via* nano-patterning of synthetic glucose dehydrogenase on spatially tunable gold nanoparticle (AuNP)-modified electrode

Hyeryeong Lee[a,1], Yoo Seok Lee[a,1], Soo Kyung Lee[b,1], Seungwoo Baek[c], In-Geol Choi[c], Jae-Hyung Jang[b], In Seop Chang[a,*]

[a] School of Earth Sciences and Environmental Engineering, Gwangju Institute of Science and Technology (GIST), 261 Cheomdan-gwagiro, Buk-gu, Gwangju 61005, Republic of Korea

[b] School of Electrical Engineering and Computer Science, Gwangju Institute of Science and Technology (GIST), 261 Cheomdan-gwagiro, Buk-gu, Gwangju 61005, Republic of Korea

[c] Department of Biotechnology, College of Life Sciences and Biotechnology, Korea University, 145 Anam-ro, Seongbuk-gu, Seoul 02841, Republic of Korea

ARTICLE INFO

Keywords:
Direct electron transfer
Enzyme nano-patterning
Immobilization
Protein agglomeration
Charge transfer resistance

ABSTRACT

In this study, the effect of inter-enzyme steric hindrance that occurs during enzyme immobilization on the electrode, on direct electrical communications of enzyme with electrode was investigated *via* nano-patterning of enzymes on the electrode. Here, the nano-patterning of enzymes was achieved through the combination of DET-capable enzyme that was produced *via* fusion of site-specific gold binding peptide (GBP) to catalytic subunit of enzyme and gold nanoparticle (AuNP) array with highly tunable dimensions of AuNPs, resulting in spatially controllable enzyme-electrode. The nano-scale spatial control between immobilized enzymes on the highly tuned AuNPs shows different DET efficiency across the enzyme-electrode interface, showing 18.47% of maximum electron recovery which is 3.2-fold enhanced electron recovery efficiency compared to spatially non-controlled enzymes on the electrode where showed 5.7% of electron recovery. The result affirms that inter-enzyme interaction is a significant parameter that decides the enzyme-electrode performance.

1. Introduction

The direct electron transfer (DET) in terms of bioelectronics is one of the most critical issues for developing bioelectrocatalysis in photosynthesis, biomass degradation, enzymatic electrosynthesis, biosensors, and biofuel cells (Guo et al., 1991; Ikeda et al., 1993; Wang, 2002; Wollenberger, 2005; Shleev et al., 2005; Lee at al, 2016; Rasmussen et al., 2016; Hatada et al., 2018). Intimate electrical coupling of enzymes with electrodes having excellent electrochemical conductance is of paramount importance for highly efficient DET, which can be achieved with following conditions; 1) the electrode material should have high electrical conductivity for easy electron acceptance (Gooding, 2005). 2) The enzyme should be stably confined at the electrode surface to retain its surface adsorption (Kim et al., 2006). 3) The substrate or product should be easily diffusible to/from the immobilized enzyme, without a diffusion barrier (Zebda et al., 2011). 4) ET distance between the enzymatic redox site and the electrode surface should be in close proximity within 20 Å (2 nm) since ET efficiency is highly dependent on electron tunneling distance (Marcus and Sutin, 1985; Leech et al., 2012; Milton et al., 2017). 5) the ET from enzymatic redox site toward electrode should not be interfered by external insulating agents which lead to increase in charge transfer resistance (R_{ct}) (Kamin and Wilson, 1980; Houseman and Mrksich, 1999; Love et al., 2005).

Over the years, many researchers have extensively studied on the above stated requirements, 1) to 3) that led to important development and recently, there has been significant progress reported focusing on the fourth requirement, *i.e.* immobilization methods for more efficient DET. For instance, 1,2-benzoquinone and ubiquinone in the PQQ-dependent glucose dehydrogenase anodes have been studied as orienting agents that provides the enzyme positioning with the PQQ facing closer to the electrode surface, enabling direct transfer of electrons from enzymatic cofactor to electrode surface (Babanova et al., 2014, 2015). In the efforts to enhance DET efficiency, gold nanoparticles or minimal

* Corresponding author.
E-mail address: ischang@gist.ac.kr (I.S. Chang).
[1] These authors contributed equally to this work.

https://doi.org/10.1016/j.bios.2018.10.013
Received 17 July 2018; Received in revised form 16 September 2018; Accepted 9 October 2018
Available online 13 October 2018
0956-5663/

Table 1
DET-based bioelectrocatalysis and performance differences at various enzyme-electrode.

Approach	Research achievement	Type of electrode	Biocatalyst (amount of enzyme used)	Current/ enzyme loading ($\mu A\ U^{-1}$)	Electrical test(s) performed: test conditions	Reference
Nafion film coating on enzyme adsorbed electrode	To prevent loss of enzyme and improve the anti-interfering ability	Nafion/GO_x/Pt/CNT	GO_x (500 U ml^{-1})	13.3	Chronoamperometry (CA) test: 41.4 $\mu A\ cm^{-2}$	Tang et al., 2004
Enzyme immobilization onto a prussian blue-modified electrode with a Nation layer	To enhance electrocatalyst for hydrogen peroxide reduction and sensitivity of enzyme-electrode	prussian blue-modified electrode	GO_x (50 U)	8.10×10^{-5}	CA test: 0.18 $\mu A\ cm^{-2}$	Karyakin et al., 1995
Incorporation of bacteriophage as biological template for nanomesh	To enhance biomolecular recognition of electrode with biomolecules and DET	GOx/PEI/SWNT-M13 nanomesh	GO_x	–	CV test: About 100 μA of peak current was obtained at *c.a.* −0.35 V (*vs.* Ag/AgCl), 400 $mV\ s^{-1}$. (Current was extracted from graph)	Lee et al., 2016
Protection of enzyme in a silica matrix and immobilization on high surface area electrode	Excellent conductivity of electrode and retained enzymatic bioactivity	Au–PPy–rGO nanocomposite	Acetylcholine sterase (500 U mg^{-1})	6.00	CA test: 0.9 $\mu A\ cm^{-2}$ was obtained at 650 mV of applied potential Cyclic voltammetry (CV) test: oxidation peak potential obtained at *c.a.* 200 mV (*vs.* Ag/AgCl)	Yang et al., 2014
The combined graphene and Pt nanoparticle as electrode	High electrical conductivity and facilitated oxidation of H_2O_2	GNS-nPt	Cholesterol oxidase (54 U mg^{-1}), cholesterolesterase (13.2 U mg^{-1})	0.43	CA test: 0.23 mA was obtained at 0.4 V of applied potential. CV test: 0.16 V of peak-to-peak separation (ΔE_p) was obtained on the GNS-nPt electrode, 100 $mV\ s^{-1}$ EIS test: 19 kΩ (R_{ct}).	Dey and Raj, 2010
Cross-linking of enzyme with Au nanoparticles	Stable immobilization of enzyme and effective electrical contact of enzyme with the electrode	bis-aniline-cross-linked GDH/AuNP composite	FAD-GDH	–	CV test: anodic current observed at −0.35 V (*vs.* Ag/AgCl), 5 $mV\ s^{-1}$.	Yehezkeli et al., 2011
The site-specific attachment of a gold nanoparticle to the enzyme	Increased electrical conductivity across enzyme-electrode interface	GO_x mutant-AuNP conjugate/ Au electrode	GO_x	–	CA test: 0.05 $\mu A\ cm^{-2}$ was shown with 0.6 V (*vs.* Ag/AgCl) of applied potential. CV test: peak current > 50 $\mu A\ cm^{-2}$ was shown at *c.a.* −0.2 V (*vs.* Ag/AgCl), 10 $mV\ s^{-1}$. Potentiostatic polarization curve: 0.25 $\mu A\ cm^{-2}$ was shown at *c.a.* 0 V of set potential. (Data was extracted from graph)	Holland et al., 2011
Adsorption of enzyme on positively charged ZnO nanorods matrix	High affinity of the negatively charged enzyme with electrode, retained bioactivity, and promoted electron transfer across enzyme-electrode interface	PDDA/ GO_x/ ZnO/ MWNTs	Go_x (2 U)	1.75	CA test: 3.49 μA of steady current was measured at *c.a.* 0.1 V of the applied potential.	Wang et al., 2009
Modification of electrode with ubiquinone or its functional analogues (1,2- and 1,4-benzoquinones)	Increased the electron transfer rate *via* creation of electron sink, on the electrode surface	PQQ-dependent GDH/ CNT paper	PQQ dependent glucose dehydrogenase	–	CV test: 50 μA of redox peak was obtained at *c.a.* 0.0 V (vs Ag/AgCl) after addition of glucose (scan rate: 150 $mV\ s^{-1}$). Potentiostatic polarization curve: N.M.(Data was extracted from graph)	Babanova et al., 2015
Inter-enzyme spacing *via* nano-patterning of synthetic enzymes on AuNP-modified electrode	Alleviation of inter-enzyme agglomeration and facilitated ET	plane Au electrode	Synthetic GDH (0.43 U)	92.74	CV test: 1.05 mA U^{-1} of peak current was obtained at *c.a.* −0.11 V (*vs.* Ag/AgCl), 50 $mV\ s^{-1}$	This study
		Au/SRS		–	CV test: Peak current stabilized after 5 scans shown to be 0.477 mA U^{-1} at *c.a.* −0.18 V (*vs.* Ag/AgCl), 50 $mV\ s^{-1}$	
		AuNP-modified electrode (AuNP: 10 nm)		297.14	CV test: 2.35 mA U^{-1} of peak current was obtained at *c.a.* −0.15 V (*vs.* Ag/AgCl), 50 $mV\ s^{-1}$	

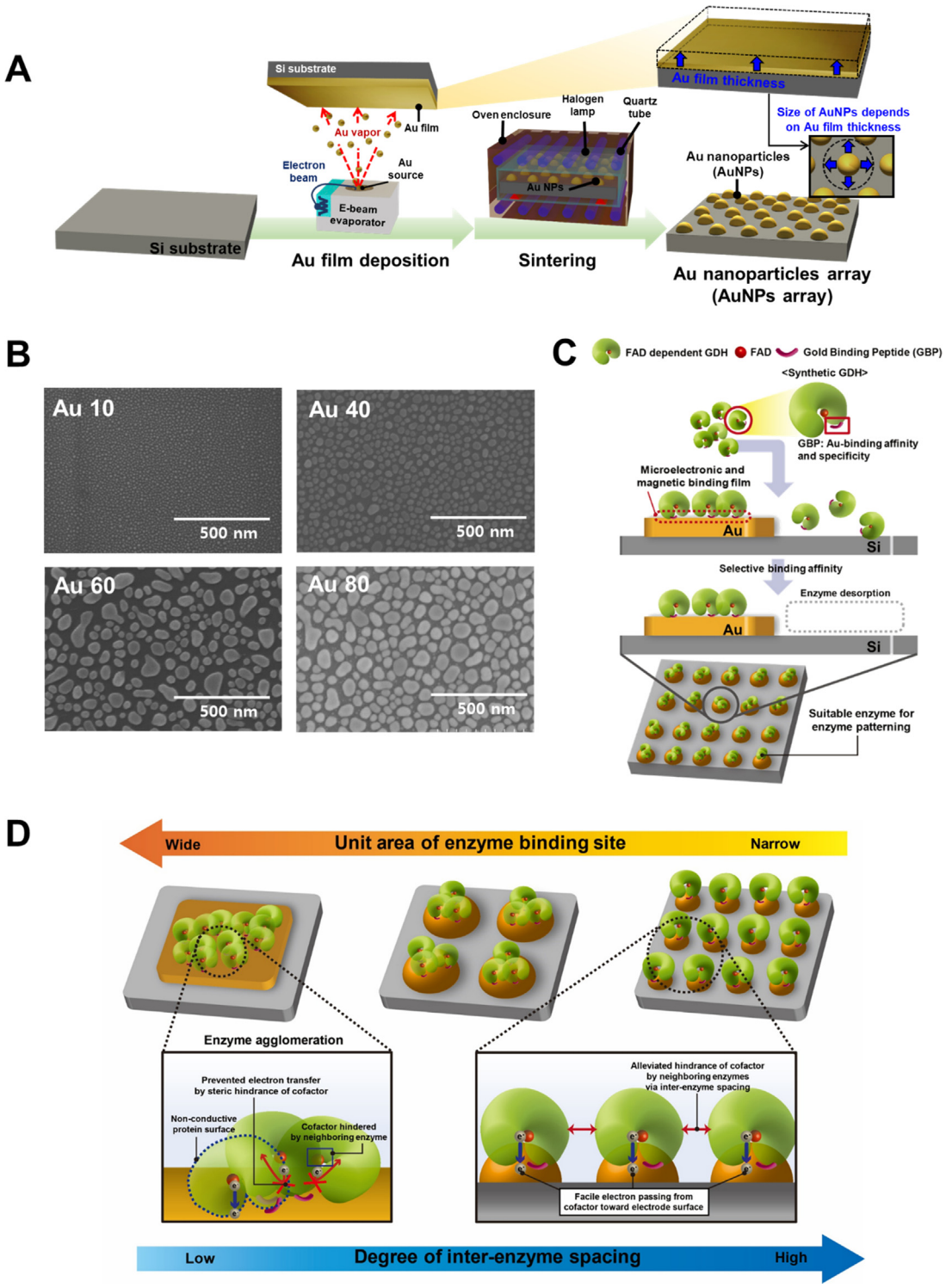

Fig. 1. Approaches for the nano-patterning of synthetic enzymes on spatially tunable gold nanoparticle (AuNP)-modified electrode. A) The fabrication process of AuNP arrays, where size of AuNPs is highly tunable, as a platform for enzyme patterning B) SEM images of fabricated AuNP arrays in different sizes of AuNPs [Note: The number next to 'Au' indicates the mean diameter (nm) of AuNPs]. C) Selective binding of synthetic enzymes on AuNPs with their desorption on bare silicon surface due to Au specific binding affinity of gold binding peptide fused to synthetic GDH. D) Steric hindrance of cofactor by neighboring enzymes followed by insulated electron transfer on plane Au (Leftmost). Enzyme patterning controlled the unit area of enzyme binding site which in turn increased the inter-enzyme spacing that significantly control the cofactor hindrance as well as facilitate electron transfer (Middle and rightmost).

cytochrome c, ET bridges, have been incorporated near the catalytic site of enzymes, providing intimate contact between the electron donor and acceptor (Holland et al., 2011; Algov et al., 2017). Recent significant advances in the development of DET-based bioelectrocatalysis are tabulated in Table 1.

However, as a matter of fact, most results show low or almost no DET signals with electrode compared to MET based signals, indicating that the number of DET-capable enzymes is limited (Arechederra et al., 2010; Walcarius et al., 2013). This limitation could be mainly due to the position of enzyme cofactor in narrow and deep cleft of enzyme causing

the enzymatic active site to have rare chance for electrical contact with electrode (Laskowski et al., 1996; Xu et al., 2004). Furthermore, ET at biocatalyst-electrode interface are insulated by protein agglomeration caused by hydrophobic interactions among proteins, led by van der Waals contacts between nonpolar regions of amino acid residues (Moreira et al., 2007). The hampered ET due to enzyme agglomeration can be explained with Eq. (1) (Rowe, 1995; Rodríguez-Valverde and Tirado-Miranda, 2009);

$$R_{ct} = \rho L/A \quad (1)$$

where, ρ is the resistivity of the material (Ω m), L is the distance separating the electron donor and acceptor (m), and A is the cross-sectional area of the electrical current (m^2). In this case of enzyme-electrode, L and A corresponds to ET distance and electrical contact area between enzymatic cofactor and electrode surface, respectively. The location of catalytic site that lies deep inside the protein structure could easily cause increase in L, ET distance, as well as increase in R_{ct}. To reduce ET distance, appropriate enzymatic orientation is usually required for close proximity between the redox cofactor and the electrode. In addition, during immobilization of large amount of enzymes on electrodes, the electrical contact area, A, could be limited due to obstruction of enzymatic cofactor by non-conductive exterior of surrounding enzymes, accompanying increase in R_{ct}. Here, it is assumed that as the enzyme-electrode interface becomes electrically less insulated, the electrons would be easily transferred across enzyme-electrode interface and the ET would become thermodynamically and kinetically favorable. As such, in this study, 1) we use the synthetic glucose dehydrogenase (GDH), consisting of the site-specific expression of a gold binding peptide (GBP) on the α-subunit of GDH which enables close proximity between enzymatic active and electrode surface as well as DET of enzyme-electrode interface (Lee et al., 2018); 2) fabricate gold-nanoislands with dimension-tunable AuNPs having diameter of 10, 20, 40, 50, 60, and 80 nm; 3) immobilize the synthetic GDH on spatially tunable AuNP array, resulting in spatially controlled immobilization of enzymes on the electrodes as well as inter-enzyme spacing; 4) investigate the relationships between the AuNP size of electrode and ET efficiency.

2. Materials and methods

2.1. Enzyme preparation

Synthetic constructs that comprises GDH α subunit and GDH γ subunit with GBP at C-terminus and GDH γ subunit, respectively, were cloned into modified pET21a plasmid and transformed to expression host *E. coli* BL21 - CodonPlus (DE3) - RIL (Agilent Technologies, USA). Then, the vectors were cultivated and the synthetic GDH was expressed and purified as previously described (Lee et al., 2018).

2.2. SPR Characterization

The binding affinities of fusion and native enzymes on gold electrodes were measured by surface plasmon resonance (SPR) using a Biacore 300 system (GE Healthcare). The data were collected using the BIA evaluation 4.1 software program. During the experiments, a baseline was established by injection of reaction buffer, followed by injection of the target analyte at a flow rate of 10 μl min^{-1} until fully charged. The buffer was then injected again to monitor dissociation behavior. The Langmuir isotherm model was used to determine kinetics of adsorption process. The apparent binding rate (k_{obs}) (s^{-1}) was calculated as $k_{obs} = k_a C + k_d$, where k_a is the association constants (M^{-1} s^{-1}), k_d is the dissociation constant (s^{-1}), and C is enzyme concentration (M). The equilibrium constant (K_{eq}) was calculated as $K_{eq} = k_a/k_d$, and the equilibrium surface coverage (θ) was determined using $\theta = C/(C + K_{eq}{}^{-1})$ (Kacar et al., 2009).

2.3. Fabrication of AuNP array

To create AuNP-modified electrodes, the Au thin film was deposited on the Si substrate using an e-beam evaporator and sintered for 1 min (Fig. 1A). The Au thin film thickness and sintering temperature were adjusted to make the AuNPs with different diameters. The sintering temperature and mean diameters of AuNPs for different Au film thickness are summarized in Table S1. The fabricated AuNP array was visualized with the scanning electron microscope (SEM, S-4700, Hitachi, Japan) (Fig. 1B). As expected, the average size of the AuNPs in each AuNP array increased with increasing deposited film thickness. To analyze the average diameter of the AuNPs, freeware image processing program (Image J 1.42q, NIH) is utilized and summarized in Table S1 as well as fabrication conditions which are the thickness of deposited gold film and annealing temperature. For the electrochemical test, geometric size of AuNP array was regulated for each AuNP array to have equal area of Au substrate (0.36 cm^2), based on information obtained from image processing program.

2.4. Electrochemical measurements

Electrochemical tests including CV, chronoamperometry, and electrochemical impedance spectroscopy (EIS), were performed using a potentiostat (Metrohm AutoLab, Utrecht, Netherlands) in the 100 mM PBS buffer (pH 7.0) containing 100 mM glucose at 30 °C. The gold electrode, Pt wire, and Ag/AgCl (3 M KCl) (MF-2052; Bioanalytical Systems Inc., West Lafayette, IN) were used as working electrode, counter electrode, and reference electrode, respectively. The CV was performed at the potential range of the working electrode from − 800–0 mV (*vs.* Ag/AgCl), at scan rates of 50 mV s^{-1} unless otherwise indicated. Chronoamperometry was tested by application of − 200 mV of continuous potential to the working electrode for 10 min. EIS test was performed under potentiostatic control in the frequency range of 0.01–1.0 × 10^5 Hz. All the experiments were conducted in duplicate.

3. Results and discussion

3.1. Direct electrochemistry of synthetic enzyme-electrode and its DET behavior depending on the enzyme-electrode interfaces

We use the synthetic GDH (GDHαCG-γNG) which comprises of GDH α subunit and GDH γ subunit that GBP is fused at C-terminus and N-terminus, respectively. Our previous result showed that the synthetic GDH (GDHαCG-γNG), in which GBP was expressed only at the catalytic subunit, the α subunit, and of the native GDHα-γ on a gold electrode, has a relatively strong DET capacity compared to other synthetic GDHs (Lee et al., 2018). It shows strong binding affinity toward gold substrate, showing 3.2-fold higher binding kinetics than that of the native GDH where GBP is absent (K_{eq} of 1.80 × 10^8 *vs.* 5.33 ×10^7). (Fig. S1) The fusion of GBP to GDH α subunit where the FAD center is located, was proven to enable DET of synthetic enzyme with electrode *via* enabling close proximity between enzymatic active site and electrode surface (Fig. 2B).

Conditions for achieving efficient DET *via* enzyme immobilization are heavily determined by the materials architecture. Conductive nanostructures (*e.g.,* Au, ZnO, carbon nanotubes (CNTs)) provide a ready means to create a 3-D, porous, conductive catalytic matrix on an electrode surface (Ding et al., 2010; Che et al., 2011; Hussein et al., 2011; Goran et al., 2013). Thereby, we fabricated Au electrode with nanoscale surface relief structures (Au/SRS) into 3 types (Fig. S2). The SEM images and structural characteristics of fabricated electrodes are shown in Fig. S3. As depicted in Fig. 2A, the synthetic GDH was incorporated onto plane Au electrode and three Au/SRSs (Au/SRS 1, Au/SRS 2, and Au/SRS 3). Then, the DET capacities of enzyme-electrodes were examined using CV and EIS (Fig. 2B and C). Following the addition of glucose, the fusion construct on plane electrode showed strong redox

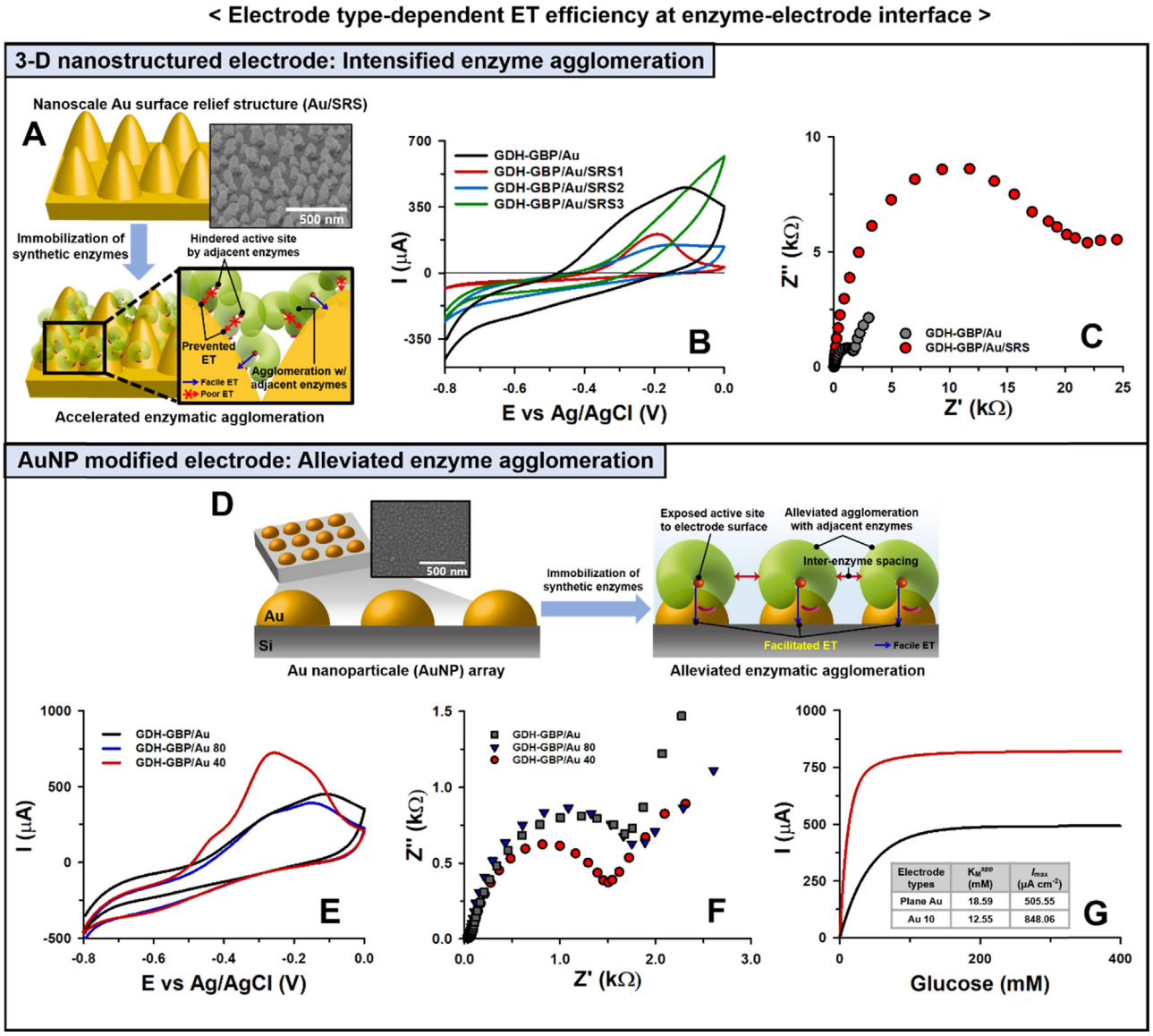

Fig. 2. The electron transfer characteristics at enzyme-electrode interface, which is dependent on surface structure of electrodes. A) Schematic showing accelerated enzymatic agglomeration on nanoscale Au surface relief structure (Au/SRS). B) CV plots of plane Au electrode and Au surface relief structures, Au/SRS 1, Au/SRS 2, Au/SRS 3, after immobilization of synthetic GDH (scan rate: 50 mV s^{-1}). C) Nyquist plots of synthetic GDH bound on plane Au electrode and Au/SRS 1. D) Schematic showing spatial tuning of synthetic enzymes on AuNP array. E) CV plot of synthetic enzyme on plane Au electrode, Au 40, and Au 80 (scan rate: 50 mV s^{-1}) and F) Nyquist plot of synthetic enzyme on plane Au electrode, Au 40, and Au 80. Applied potential is open circuit potential. G) Plot of I_{max} of synthetic enzyme on plane Au electrode (black) and Au 10 (red) as a function of glucose concentration, where I_{max} is obtained from CV data (Inset: K_M^{app} and I_{max} of synthetic enzyme on a plane Au electrode and Au 10). (For interpretation of the references to color in this figure legend, the reader is referred to the web version of this article.)

events at −455 mV (*vs.* Ag/AgCl). The increase in the oxidative current is a response to enzyme-catalyzed glucose oxidation. The starting potential of −455 mV provided evidence for efficient DET between the FAD center and the electrode, which had a formal potential ($E^{\circ\prime}$) of −450 mV (*vs.* Ag/AgCl) at pH 7.0 (25 °C) (Lu et al., 1994; Katz et al., 2004; Holland et al., 2011). The fusion constructs on nano-modified electrodes shows overpotential in oxidative reaction *c.a.* 100 mV, therefore, a response to enzyme-catalyzed glucose oxidation starting at *c.a.* −380 mV (*vs.* Ag/AgCl). Moreover, it was found that the voltammogram of synthetic GDH at three modified ones (*i.e.,* Au/SRS 1, Au/SRS 2, and Au/SRS 3) has shown diverse tendency in the respect of peak current, catalytic potential and voltammogram shape. The catalytic current of synthetic enzyme at the Au/SRS 1 and Au/SRS 2 was highly reduced compared with the plane Au electrode and flattening of the voltammetric waves has occurred in concert with decrease in peak current at the synthetic enzyme on the Au/SRS 2. Also, extreme shift of peak potential in positive direction was shown at the synthetic GDH on the Au/SRS 3, where the current has exceeded the value of synthetic GDH on plane Au electrode from *c.a.* −100 mV (Fig. 2B). Even at the EIS measurement, the R_{ct} of synthetic enzyme on the Au/SRS 1 is an order of magnitude greater than on the plane electrode (Fig. 2C). It is unexpected results that the ET conditions of DET-based enzymes was not favorable on high surface area electrode, which is different phenomenon compared with MET-based high-active electrode (Vazquez-Duhalt et al., 2014; Do et al., 2015). It is assumed that enzymes on Au/SRS which has uneven surface tends to immobilize in an irregular manner, causing intensified inter-enzyme agglomeration.

3.2. Nano-patterning of synthetic enzymes on AuNP-modified electrode and its effect on DET property of enzyme-electrode

Therefore, DET efficiency of enzyme-electrode depending on

external insulating agent was investigated *via* nano-patterning of synthetic enzymes on highly tuned modified electrode (Figs. 1D and 2D). This approach is based on the idea that ET at enzyme-electrode interface was hampered due to shielding of enzymatic active site by protein shell of neighboring enzyme and spatial tuning of enzymes on AuNP array would enable control of cofactor hindrance by adjacent enzymes (Fig. 1D). The selective binding property of synthetic enzymes on AuNPs enabled enzymatic nano-patterning in accordance with AuNP patterns on the electrode (Fig. 1C). At the fabrication step of AuNP arrays, the unit size of AuNPs was controlled to regulate number of enzymes immobilized per AuNP.

The synthetic GDH was immobilized on highly tuned AuNP electrodes, Au 10, Au 20, Au 40, Au 50, Au 60, Au 80, and electrochemical test was conducted to investigate reaction mechanisms, electron transfer kinetics with redox reaction potential and current densities of synthetic GDH-electrode. The results show that immobilization of enzymes on AuNP arrays with different diameters results in different enzyme-electrode interface conditions for DET. The DET capacities were examined using CV (Fig. 2E, Figs. S5–S11). Following the addition of glucose, all types of fusion construct-electrode showed strong redox events. The catalytic current starting potential of Au 40 is *c.a.* − 460 mV provided evidence for efficient DET between the FAD center and the electrode, which is very close to a formal potential ($E^{\circ\prime}$) of −450 mV (*vs.* Ag/AgCl) at pH 7.0 (25 °C). However, the catalytic current starting potential of enzyme-electrodes shifted positively with the AuNP diameter order (the smaller, the higher); the oxidation current starting potential of Au 80 is shifted by 50 mV in a positive direction and the maximum oxidation current obtained at *c.a.* −150 mV (*vs.* Ag/AgCl) is 2.0 times lower than those of Au 40.

The peak current obtained from CV was then plotted according to glucose concentration of 0–400 mM to estimate the apparent kinetic parameters of synthetic enzyme on Au 10 and plane Au electrodes (Fig. 2G). Using the linear part of the transient curves and a Lineweaver-Burk transformation, the electrochemical K_M^{app} and I_{max} values in the Lineweaver-Burk plot were calculated. The electrochemical K_M^{app} was calculated with 12.55 and 18.59 mM for synthetic GDH on Au 10 and plane Au electrode, indicating that the synthetic GDH on Au 10 has higher affinity for glucose, compared to plane Au electrode. Moreover, the I_{max} was 1.68-fold higher for the synthetic GDH on Au 10 than on the plain Au electrode (848.06 μA cm^{-2} *vs* 505.55 μA cm^{-2}), indicating that the spatial control of synthetic enzyme on AuNPs array could render favorable condition for interfacial DET at enzyme electrode, preventing the hindrance of cofactor by neighboring protein shells.

Then, the amperometric response of synthetic enzyme immobilized Au 10, Au 20, Au 40, Au 50, Au 60, Au 80, and plane Au electrode was obtained under the assumption that DET condition at enzyme-electrode interface would vary depending on controlled inter-enzyme spacing and position (Fig. 3A). The amperometric response of enzyme-electrode showed its steady-state current after 3 min. The current of synthetic enzymes on plane Au electrode, Au 50, Au 60, Au 80 shows similar current values, showing 39.88, 37.16, 28.19, 46.51 μA, respectively. However, when the mean diameter of AuNPs become < 40 nm, the response currents increase apparently according to decrease in mean diameter of AuNPs, showing 66.88 μA, 89.71 μA, and 127.77 μA for Au 40, Au 20, and Au 10, respectively. The amperometric results were then used to obtain the efficiency of electron recovery *via* comparison of measured current and theoretical current obtained from the used enzyme mass and the specific activity of used enzyme. The electron recovery of synthetic enzyme on Au 10, Au 20, Au 40, Au 50, Au 60, Au 80, and plane Au electrode were shown to be 18.5, 12.9, 9.67, 5.37, 4.08, 4.65, 5.67%, respectively, showing 3.2-fold enhanced efficiency at Au 10 compared to plane Au electrode.

The R_{ct} of the synthetic enzyme immobilized Au 10, Au 20, Au 40, Au 50, Au 60, Au 80, and plane Au electrode was determined by EIS to analyze DET conditions at the enzyme-electrode interfaces. The R_{ct} of synthetic enzymes on AuNP arrays and plane Au electrode is shown to increase with increase in pattern size (Figs. 2F and 3B); Here, plane Au electrode was assumed to have the largest Au pattern size. The increase in interfacial R_{ct} of enzyme-electrode indicates that the electronic conductivity between electron donor and electrode become reduced, resulting that interfacial ET of enzyme-electrode become sluggish which is related to reduction in ET kinetics. This result is in agreement with the hypothesis that the R_{ct} of enzyme-electrode interface is significantly dependent on the pattern size of AuNPs array, because increase in R_{ct} at enzyme-electrode interface is highly ascribable to inter-enzyme lateral crowding that is intensified with increase in pattern size of AuNP array. The R_{ct} was measured to increase gradually as mean diameter of AuNPs increases and show similarity as mean diameter of AuNPs get > 40 nm, showing 969.14, 1155.1, 1726.0, 1948.0, 2064.0, 2124.0, and 2265.6 Ω at synthetic enzymes with Au 10, Au 20, Au 40, Au 50, Au 60, Au 80, and plane Au electrode, respectively.

3.3. Quantification of electroactive enzymes on the plane Au electrode and spatially tunable electrode

After incubating synthetic enzyme for different adsorption time, the surface coverage (θ) of the enzymes on the electrode as well as R_{ct} for interfacial ET between enzyme and electrode were estimated at different incubation time (Fig. 3C). From the obtained data, the number of electroactive enzymes which are effectively involved in interfacial ET of enzyme-electrode was then determined as well as the ratio of electroactive enzymes to the total enzyme immobilized on the electrode.

Estimation of enzyme surface coverage on plane Au electrode and Au 10 was followed by EIS measurement of ferri-/ferrocyanide redox system in the PBS buffer (100 mM) containing 10 mM $Fe(CN)_6^{3-}$ and 10 mM $Fe(CN)_6^{4-}$, under potentiostatic control at a potential of + 230 mV *vs.* Ag/AgCl. It is usually assumed that the electron communication between redox probe and the electrode increasingly obstructed with the increase in enzymatic coverage because the redox species do not penetrate the highly organized enzymatic layer formed on the electrode surface. From the EIS results, the surface coverage can be derived from the Eq. (2) (Dowd and Riggs, 1965; Wang et al., 2005)

$$\theta = 1 - R_{ct}^{network}/R_{ct}^{enzyme} \quad (2)$$

where, $R_{ct}^{network}$ (Ω) denotes the charge transfer resistance of the bare gold electrode and R_{ct}^{enzyme} (Ω) is the corresponding resistance of the electrode passivated along with adsorption of synthetic enzyme. At the beginning, the average surface coverage of enzyme rapidly increased and then it reached a stable value of 86.3 after 120 min of incubation time, with relative standard deviation of 0.05–6.0%.

In parallel, the R_{ct} for interfacial ET between enzyme and electrode was measured for synthetic enzymes immobilized plane Au electrode and Au 10, with different adsorption time. The interfacial R_{ct} at the enzyme-electrode was measured as surface coverage of enzyme on the electrode increased, in other words, the number of electron donor (*i.e.,* enzymatic cofactor) increased on the electrodes. The R_{ct} of both enzyme-electrodes significantly decreases with the increase in enzymatic coverage on the electrode, implying that highly conductive DET-based enzyme-electrode was developed after immobilization of synthetic enzymes on plane Au electrode and Au 10. However, as incubation time increases, their R_{ct} exhibit different EIS profile where the synthetic enzyme on plane Au electrode is reaching 2632.2 Ω, while synthetic enzyme on Au 10 decreases continuously reaching 1130.0 Ω; in this case, the surface coverage of enzyme is 87.23%. Here, the results show that the relative standard deviation is 2.0–27% for synthetic enzyme on plane Au electrode while synthetic enzyme on Au 10 shows 1.0–20% of relative standard deviation. Reduction in R_{ct} indicates that the number of transferred electrons from electron donors to electrodes become increased, which means the number of electroactive enzymes has increased. In addition, significant disparity in R_{ct} of synthetic enzymes on Au 10 and plane Au electrode was recorded even at enzymatic coverage

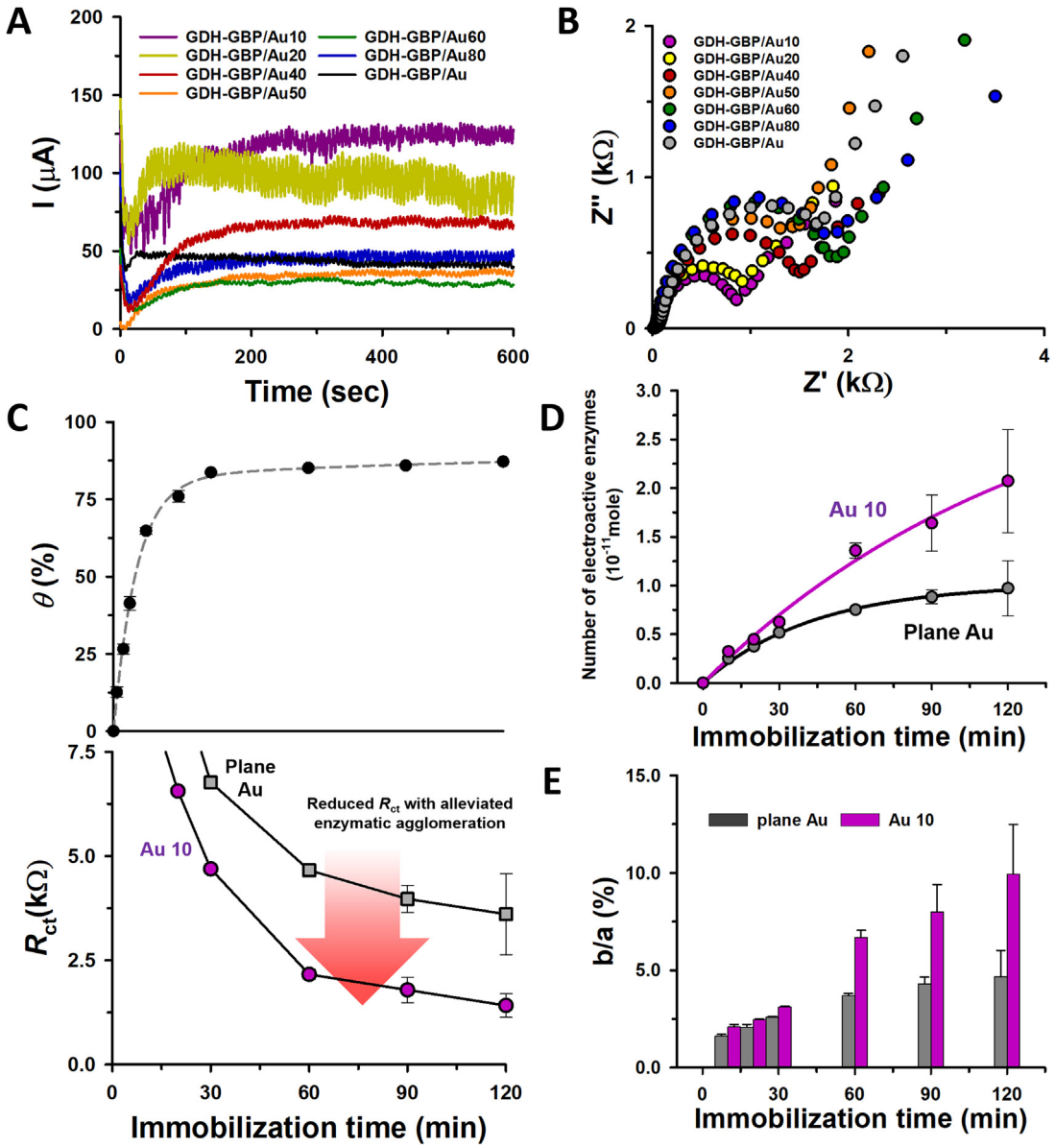

Fig. 3. Electrochemical properties of synthetic enzymes on spatially tunable gold nanoparticle (AuNP)-modified electrode. A) Amperometric responses of an enzyme-bound Au 10, Au 20, Au 40, Au 50, Au 60, Au 80, and plane Au electrode. (applied potential: −200 mV *vs.* Ag/AgCl). B) Nyquist plots of synthetic enzymes on Au 10, Au 20, Au 40, Au 50, Au 60, Au 80, and plane Au electrode at immobilization time of 2 h. Open circuit potential was applied. C) Surface coverage of enzymes (black, circle) according to immobilization time (top) (relative standard deviation (RSD) = 0.05–6.0%), and R_{ct} change at plane Au electrode (grey, square) (RSD = 2.0–26%) and Au 10 (purple, circle) during 120 min of enzyme immobilization (bottom) (RSD = 1.0–21%) D) Number of electroactive enzymes which effectively transfer electrons to the electrode, on the plane Au electrode (RSD = 2.0–27%) and Au 10, according to incubation time of enzymes. (RSD = 1.0–20%) E) Ratio of electroactive enzymes (b) and actually immobilized enzymes (a) on plane Au electrode (RSD = 2.0–27%) and Au 10 (RSD = 1.0–20%), according to incubation time of enzymes (The ratio was described as 'b/a'). (For interpretation of the references to color in this figure legend, the reader is referred to the web version of this article.)

below 80%. It was seen that the interfacial ET from enzymatic cofactor to electrode is more likely to be interfered on the plane Au electrode where cofactor hindrance by neighboring enzymes is prone to occur compared with Au 10 where enzyme binding site of electrode is spatially controlled. This indicates that the increase in R_{ct} of enzyme-electrode interface is highly associated with enzymatic agglomeration.

Then, the number of electroactive enzymes which are the enzymes that effectively involved in interfacial ET of enzyme-electrode was determined from the R_{ct} of enzyme-electrode at different immobilization time. Furthermore, the ratio of the number of electroactive enzyme and total enzymes immobilized on the electrode was evaluated with time using measured surface coverage θ as well as R_{ct} of enzyme-electrode. The number of electroactive enzymes was derived from the Eq. (3) (Alfonta et al., 2000; Katz and Willner, 2003; Shervedani et al., 2006).

$$R_{ct} = RT \times (n^2F^2Ak_{et}[S])^{-1} \quad (3)$$

where, R is the ideal gas constant, T is the temperature (K), n is the number of transferred electrons per one molecule of enzyme, F is Faraday's constant, A is surface area of the electrode (cm^2), k_{et} is charge transfer rate constant (s^{-1}) and [S] corresponds to the concentration of the electroactive enzymes (mol cm^{-2}). The dependence of redox peak potentials on the scan rates from 10 to 100 mV s^{-1} was utilized to derive the k_{et} values, based on Laviron's model (Eckermann et al., 2010; Laviron, 1979; Zhang et al., 2015) (Figs. S5 and S8b). From the Laviron's equation, the k_{et} could be obtained as 1.93 and 2.31 s^{-1} for synthetic enzymes on plane Au electrode and Au 10, respectively.

The Fig. 3D shows the number of electroactive enzymes against immobilization time is plotted for synthetic enzyme on plane Au electrode and Au 10 (Fig. 3D). At the enzymatic coverage of < 75.96%, the synthetic enzyme immobilized plane Au electrode and Au 10 showed similar number of electroactive enzymes as well as the ratio of electroactive enzymes to the total immobilized enzymes. This indicates that the two electrodes formed similar interfacial ET conditions for enzyme-electrode. However, for plane Au electrode, the margin of increase in number of electroactive enzymes drops after additional enzyme loading, while the number of electroactive enzymes on Au 10 continues to increase, thus causing huge difference in the number of electroactive enzymes with that of plane Au electrode. Based on Fig. 3E, at the coverage of 87.23%, the ratio of electroactive enzyme to total immobilized enzymes on Au 10 was calculated to be 2.13 times higher than on plane Au electrode. This indicates that ET process at enzyme-electrode interface becomes kinetically favorable at nano-patterned enzyme-electrode, rendering electroactivity of immobilized enzyme molecules is enhanced. The increase in the ratio of electroactive enzymes to total immobilized enzymes implies that more number of enzymes can effectively contribute to electron delivery from enzymatic cofactor to electrode, enhancing DET efficiency. This result demonstrates that nano-patterning of synthetic enzymes on the spatially tunable AuNP array reduces enzymatic agglomeration as opposed to the plane Au electrode where higher enzymatic agglomeration clearly reduces the number of electroactive enzymes, retarding electroactive ability of enzymes. These findings provided us with a great deal of information that enzymatic agglomeration which is interrelated with R_{ct} of enzyme-electrode is a critical parameter that determines the ratio of electroactive enzymes to the total enzyme immobilized, which in turn determines the efficiency of DET.

4. Conclusion

This study aims to optimize the nano-environment of enzyme-electrode interfaces to enable efficient DET, *via* controlling inter-enzyme interactions that brings about inter-enzyme agglomeration as well as severe drop in ET efficiency. To reduce inter-enzyme agglomeration and provide favorable condition for DET in the enzyme-electrode, nano-patterning of enzymes was implemented through the combination of synthetic enzymes genetically fused with GBP and AuNP array with highly tunable dimensions of AuNPs. During the formation of nano-patterned enzyme-electrode, moreover, the diameter of AuNPs on the AuNP array was tuned in the range of 10–80 nm and the influence of inter-enzyme agglomeration on ET efficiency was electrochemically investigated with comparison of each types of nano-patterned enzyme-electrodes. The R_{ct} during ET process between enzymatic cofactor and electrode was shown to sharply reduce as pattern size of nano-patterned enzyme-electrode diminishes below 40 nm. Along with decrease in overpotential for driving interfacial DET process, the redox potential of FAD cofactor was measured to be very close to theoretical redox potential of FAD. Hence, the quantification of electroactive coverage shows that the ratio of electroactive coverage in the nano-patterned enzyme-electrode was 2.13-fold enhanced compared with non-patterned one.

This investigation provides the important information that inter-enzyme agglomeration is one of the critical parameters that might render DET process thermodynamically and kinetically unfavorable. In addition, it is implied that the spatially controlled immobilization of enzyme on the electrode could solve the problematic situation during DET by alleviating inter-enzyme spatial hindrance. These results may lead to new and important insights into the development of enzyme-based bioelectronics such as enzyme-based electrosynthesis, bio-photoelectrochemical systems, biosensors and biofuel cells, in which DET between enzyme and electrode is of main interest. Furthermore, it should be noted that further fundamental study for interfacial DET in enzyme-electrode system is crucial to significantly elevate DET efficiency, since the electroactive coverage is yet to be maximum 9.93% in this study and there is still room for improvement of ET efficiency.

Acknowledgements

H. Lee, Y. S. Lee and S. K. Lee contributed equally. This work was supported by grants from the National Research Foundation of Korea (NRF), funded by the Korean Government (2016R1A2B3015426)

Appendix A. Supporting information

Supplementary data associated with this article can be found in the online version at doi:10.1016/j.bios.2018.10.013.

References

Alfonta, L., Katz, E., Willner, I., 2000. Anal. Chem. 72, 927.
Algov, I., Grushka, J., Zarivach, R., Alfonta, L., 2017. J. Am. Chem. Soc. 139, 17217.
Arechederra, M.N., Jenkins, C., Rincón, R.A., Artyushkova, K., Atanassov, P., Minteer, S.D., 2010. Electrochim. Acta 55, 6659.
Babanova, S., Matanovic, I., Atanassov, P., 2014. ChemElectroChem 1, 2017.
Babanova, S., Matanovic, I., Chavez, M.S., Atanassov, P., 2015. J. Am. Chem. Soc. 137, 7754.
Che, A.-F., Germain, V., Cretin, M., Cornu, D., Innocent, C., Tingry, S., 2011. New J. Chem. 35, 2848.
Dey, R.S., Raj, C.R., 2010. J. Phys. Chem. C. 114, 21427.
Ding, S.-N., Holzinger, M., Mousty, C., Cosnier, S., 2010. J. Power Sources 195, 4714.
Do, T., Varničić, M., Flassig, R., Vidaković-Koch, T., Sundmacher, K., 2015. Bioelectrochemistry 106, 3.
Dowd, J.E., Riggs, D.S., 1965. J. Biol. Chem. 240, 863.
Eckermann, A.L., Feld, D.J., Shaw, J.A., Meade, T.J., 2010. Coord. Chem. Rev. 254, 1769.
Gooding, J.J., 2005. Electrochim. Acta 50, 3049.
Goran, J.M., Mantilla, S.M., Stevenson, K.J., 2013. Anal. Chem. 85, 1571.
Guo, L.-H., Allen, H., Hill, O., 1991. Advances in Inorganic Chemistry 36. Elsevier, pp. 341.
Hatada, M., Loew, N., Inose-Takahashi, Y., Okuda-Shimazaki, J., Tsugawa, W., Mulchandani, A., Sode, K., 2018. Bioelectrochemistry 121, 185.
Holland, J.T., Lau, C., Brozik, S., Atanassov, P., Banta, S., 2011. J. Am. Chem. Soc. 133, 19262.
Houseman, B.T., Mrksich, M., 1999. Angew. Chem. -Int. Ed. 38, 782.
Hussein, L., Rubenwolf, S., Von Stetten, F., Urban, G., Zengerle, R., Krueger, M., Kerzenmacher, S., 2011. Biosens. Bioelectron. 26, 4133.
Ikeda, T., Kobayashi, D., Matsushita, F., Sagara, T., Niki, K., 1993. J. Electroanal. Chem. 361, 221.
Kacar, T., Zin, M.T., So, C., Wilson, B., Ma, H., Gul-Karaguler, N., Jen, A.K.Y., Sarikaya, M., Tamerler, C., 2009. Biotechnol. Bioeng. 103, 696.
Kamin, R.A., Wilson, G.S., 1980. Anal. Chem. 52, 1198.
Karyakin, A., Gitelmacher, O.V., Karyakina, E.E., 1995. Anal. Chem. 67, 2419.
Katz, E., Sheeney-Haj-Ichia, L., Willner, I., 2004. Angew. Chem. -Int. Ed. 43, 3292–3300.
Katz, E., Willner, I., 2003. Electroanalysis 15, 913.
Kim, J., Jia, H., Wang, P., 2006. Biotechnol. Adv. 24, 296.
Laskowski, R.A., Luscombe, N.M., Swindells, M.B., Thornton, J.M., 1996. Prot. Sci. 5, 2438.
Laviron, E., 1979. J. Electroanal. Chem. 101, 19.
Lee, Y.S., Baek, S.W., Lee, H., Reginald, S.S., Kim, Y., Kang, H., Choi, I.-G., Chang, I.S., 2018. ACS Appl. Mater. Interfaces 10, 28615.
Lee, S.W., Lee, K.Y., Song, Y.W., Choi, W.K., Chang, J., Yi, H., 2016. Adv. Mater. 28, 1577.
Leech, D., Kavanagh, P., Schuhmann, W., 2012. Electrochim. Acta 84, 223.
Love, J.C., Estroff, L.A., Kriebel, J.K., Nuzzo, R.G., Whitesides, G.M., 2005. Chem. Rev. 105, 1103.
Lu, S.-Y., Li, C.-F., Zhang, D.-D., Zhang, Y., Mo, Z.-H., Cai, Q., Zhu, A.-R., 1994. J. Electroanal. Chem. 364, 31.
Marcus, R.A., Sutin, N., 1985. Biochim. Biophys. Acta Bioenergy 811, 265.
Milton, R.D., Minteer, S.D., 2017. J. R. Soc. Interface 14, 20170253.
Moreira, I.S., Fernandes, P.A., Ramos, M.J., 2007. Proteins 68, 803.
Rasmussen, M., Abdellaoui, S., Minteer, S.D., 2016. Biosens. Bioelectron. 76, 91.
Rodríguez-Valverde, M.Á., Tirado-Miranda, M., 2009. Eur. J. Phys. 30, L47.
Rowe, D.M., 1995. CRC Handbook of Thermoelectrics. CRC Press, Boca Raton, FL.
Shervedani, R.K., Mehrjardi, A.H., Zamiri, N., 2006. Bioelectrochemistry 69, 201.
Shleev, S., Tkac, J., Christenson, A., Ruzgas, T., Yaropolov, A.I., Whittaker, J.W., Gorton, L., 2005. Biosens. Bioelectron. 20, 2517.
Tang, H., Chen, J., Yao, S., Nie, L., Deng, G., Kuang, Y., 2004. Anal. Biochem. 331, 89.
Vazquez-Duhalt, R., Aguila, S.A., Arrocha, A.A., Ayala, M., 2014. ChemElectroChem 1, 496.
Walcarius, Minteer, S.D., Wang, J., Lin, Y., Merkoçi, A., 2013. J. Mater. Chem. B 1, 4878.
Wang, J., 2002. Sens. Update 10, 107.
Wang, C., Yang, C., Song, Y., Gao, W., Xia, X., 2005. Adv. Funct. Mater. 15, 1267.
Wang, Y.-T., Yu, L., Zhu, Z.-Q., Zhang, J., Zhu, J.-Z., Fan, C.-h., 2009. Sens. Actuator B-Chem. 136, 332.
Wollenberger, U., 2005. Compr. Anal. Chem. 44, 65.
Xu, X., Zhao, J., Xu, Z., Peng, B., Huang, Q., Arnold, E., Ding, J., 2004. J. Biol. Chem. 279, 33946.
Yang, Y., Asiri, A.M., Du, D., Lin, Y., 2014. Analyst 139, 3055.
Yehezkeli, Tel-Vered, R., Raichlin, S., Willner, I., 2011. ACS Nano 5, 2385.
Zebda, C. Gondran, Le Goff, A., Holzinger, M., Cinquin, P., Cosnier, S., 2011. Nat. Commun. 2, 370.
Zhang, W., Zheng, J., Tan, C., Lin, X., Hu, S., Chen, J., You, X., Li, S., 2015. J. Mater. Chem. B 3, 217.